nucleon pairs and since the mean free path of a meson at their energies was found to be less than a meson Compton wavelength, it is not at all clear that meson production and reabsorption is not just another way of describing a photon-nucleon pair interaction. If the complete process is described by $\gamma+2$ nucleons $\rightarrow 2$ nucleons, then there should be selection rules operating which will strongly favor the two nucleons being a neutron and a proton. If the process is described by a mean-free-path argument as $\gamma+$ nucleon $\rightarrow\pi+$ nucleon, $\pi+2$ nucleons $\rightarrow 2$ nucleons, then the two processes would be independent; a π^+ meson could be produced and subsequently reabsorbed by a proton-neutron pair, giving rise, finally, to a pair of correlated fast protons. Proton-proton pairs from the photodisintegration of complex nuclei have been looked for and found only in very small numbers.[17]

ACKNOWLEDGMENTS

The authors would like to thank Dr. Van Nicolai for his operation of the liquid gas target and Mr. R. Harber and Mr. R. C. Herndon for their assistance in various phases of the experimental work. Helpful discussions with G. Ascoli, G. Bernardini, G. F. Chew, and D. G. Ravenhall are also gratefully acknowledged. Thanks are also due A. Wattenberg and V. Z. Peterson for information on their work prior to publication.

[17] Weinstein, Odian, Stein, and Wattenberg, Phys. Rev. **99**, 1620 (1955). J. R. Palfrey, Photonuclear Conference, Case Institute of Technology, Cleveland, Ohio, May, 1955 (unpublished).

PHYSICAL REVIEW VOLUME 110, NUMBER 5 JUNE 1, 1958

Form Factor of the Photopion Matrix Element at Resonance*

W. K. H. PANOFSKY AND E. A. ALLTON
High-Energy Physics Laboratory, Stanford University, Stanford, California
(Received February 6, 1958)

The inelastic scattering of electrons in hydrogen leading to pion formation has been examined. Measurements were carried out in which a hydrogen target was bombarded by electrons of energy E_1 w' h secondary electrons of energy E_2 being detected by a magnetic analyzer at a fixed angle of 75°. The enc ies E_1 and E_2 were programed together such that the pions were produced at a constant energy near the peak of the pion-nucleon resonance in the $(\frac{3}{2},\frac{3}{2})$ state; at the same time the momentum transfer to the pion-nucleon system was varied. Special procedures were developed to eliminate contributions from competing processes. Approximately three fourths of the observed cross section corresponds to magnetic-dipole absorption of the incident virtual photon; the momentum transfer dependence can be interpreted in terms of a form factor of the difference between the magnetic moments of the neutron and proton. If the electron-scattering radii are assumed for the proton, then the data appear to require an rms radius of the magnetic moment of the neutron of about 1.1×10^{-13} cm, based on an exponential model; nucleon recoil corrections are still somewhat uncertain.

I. INTRODUCTION

A. General

IN a series of earlier papers[1–3] we have described our study of the direct production of π mesons in inelastic electron-proton collisions. In the previous experiments the π^+-meson yield from the reaction

$$e+p\rightarrow n+\pi^++e' \qquad (1)$$

was measured and compared with the yield from the photopion process

$$\gamma+p\rightarrow n+\pi^+; \qquad (2)$$

i.e., the yields of π^+ mesons from protons bombarded by real and virtual photons have been compared. The inelastic scattering reaction (1) and the photoproduction process (2) are nearly equivalent with the following basic difference: the interaction Hamiltonian of (2) is the product of the purely transverse photon vector potential with the current operator of the meson-nucleon current, while the corresponding Hamiltonian of (1) is the product of the Møller potential corresponding to the initial and final electron states times the meson-nucleon current. This general fact has the following consequences: (a) In the photoprocess the energy transfer to the nucleon-meson system is equal to the momentum transfer; in the electron process the energy transfer and the momentum transfer can be independently controlled by proper choice of the electron-scattering kinematics. (b) Longitudinal matrix elements can contribute to (1) but not to (2).

In our previous experiments[1–3] the quantitative significance of these effects was very difficult to establish. The reason for this problem is that the Møller potential favors electron-scattering processes where the final electron is directed in the forward direction; for

* Supported in part by the joint program of the Office of Naval Research, the U. S. Atomic Energy Commission, and the U. S. Air Force, Office of Scientific Research.
[1] Panofsky, Newton, and Yodh, Phys. Rev. **98**, 751 (1955).
[2] Panofsky, Woodward, and Yodh, Phys. Rev. **102**, 1392 (1956).
[3] G. B. Yodh and W. K. H. Panofsky, Phys. Rev. **105**, 731 (1957).

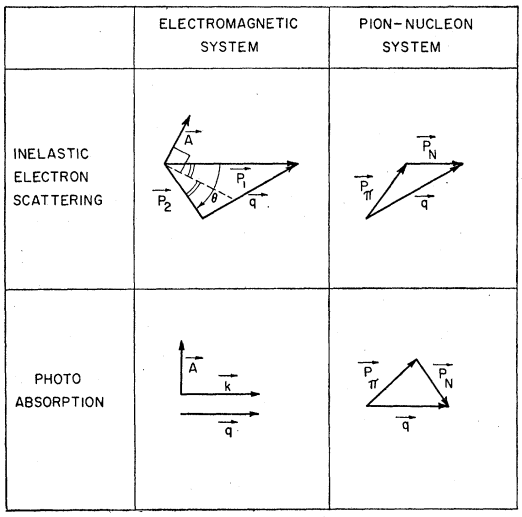

FIG. 1. Vector diagram showing the production of mesons by inelastic electron scattering and by photoproduction. Shown are the following quantities: meson momentum $\mathbf{p}_\pi$, nucleon recoil momentum $\mathbf{p}_N$, momentum transfer $\mathbf{q}$, the vector potential $\mathbf{A}$ for both processes, the initial and final momenta $\mathbf{p}_1$ and $\mathbf{p}_2$ in electron scattering, and the photon momentum $\mathbf{k}$ in photoproduction.

exact forward scattering the correspondence between processes (1) and (2) is exact (if the electron rest mass can be neglected), and therefore no information on the specific effects (a) and (b) results. Hence only the relatively small contribution from large-angle electron scattering carries any information beyond verification

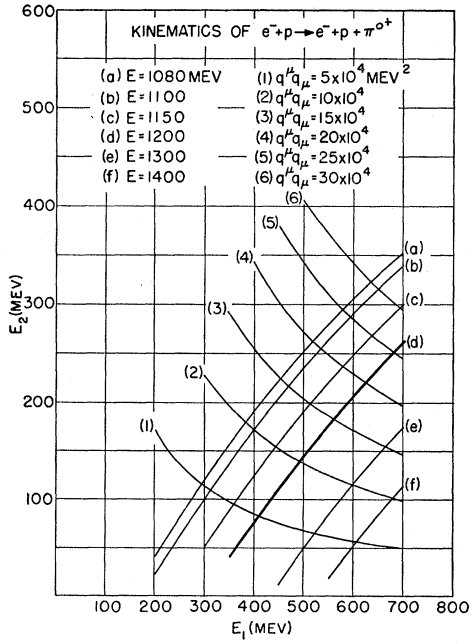

FIG. 2. Curves of constant c.m. energy E and constant invariant momentum transfer $q^\mu q_\mu$ as a function of initial and final electron energies E_1 and E_2.

of the purely electrodynamic assumptions. It became clear early in the previous work that it would be necessary to single out large-angle scattering events in order to investigate the property of the relevant matrix elements "off the energy shell," i.e., at momentum transfers exceeding the energy transfer.

The experiments described here are concerned with this problem. Inelastically scattered electrons are observed at a laboratory scattering angle of $\theta=75°$ under conditions of electron energies to correspond to pion production. The pions are not observed directly; a coincidence experiment observing both pions and electrons appears difficult.

B. Kinematics

In the experiment described here the initial electron energy (energy E_1, momentum $\mathbf{p}_1$) and the final electron energy and angle (energy E_2, momentum $\mathbf{p}_2$) are controlled. This fixes the momentum transfer

$$\mathbf{q}=\mathbf{p}_1-\mathbf{p}_2 \tag{3}$$

to the meson-nucleon system, as well as the total energy E of the meson-nucleon system in their center-of-mass frame which can be shown to be given by the relation

$$E^2=M^2-2E_1E_2(1-\cos\theta)+2(E_1-E_2)M, \tag{4}$$

where M is the nucleon mass and where the electron rest mass has been neglected. (We use units such that $\hbar=c=1$.) Equations (3) and (4) thus fix both the energy and momentum transfers; in the equivalent case of bombardment by a photon of energy k, we have simply

$$\mathbf{q}=\mathbf{k};\quad E^2=M^2+2kM. \tag{5}$$

Hence the kinematical conditions in inelastic electron scattering are identical to those in an experiment in which the sums of the total cross sections of π^+ and π^0 production were measured. Figure 1 shows the kinematical situation graphically; photoprocesses and electron processes are compared which yield the same value of E but operate under different conditions of momentum transfer.

The quantity describing the behavior of the matrix elements covariantly if the energy transfer E_1-E_2 and the momentum transfer $\mathbf{p}_1-\mathbf{p}_2$ differ, is the four-momentum transfer $q^\mu=(\mathbf{p}_1-\mathbf{p}_2, E_1-E_2)$; its magnitude is given by

$$\begin{aligned} q^\mu q_\mu &= 2(E_1E_2-p_1p_2\cos\theta-m^2) \\ &= M^2-E^2+2(E_1-E_2)M, \end{aligned} \tag{6}$$

where m is the electron rest mass; if m can be neglected, then

$$q^\mu q_\mu=2E_1E_2(1-\cos\theta). \tag{7}$$

Figure 2 describes the relations governing E and $q^\mu q_\mu$ as a function of E_1 and E_2 at a fixed electron angle $\theta=75°$. The curves in this figure have been computed using the approximate relation Eq. (7).

This experiment has been programmed such that we follow the line $E=1200$ Mev in Fig. 2, i.e., such that the energy of the fixed pion-nucleon system is constant; this energy is the same as that produced by a real photon of laboratory energy $k=298$ Mev, and is very near the maximum of the experimental pion photoproduction cross section.[4,5] The experimentally determined cross section $d^2\sigma/d\Omega dE_2$ thus traces the behavior of the photopion resonance matrix element away from the energy shell ($q^\mu q_\mu=0$).

Because of the finite value of the rest mass of the electron, the energy shell $q^\mu q_\mu=0$ cannot be quite reached; Fig. 3 shows the exact relation computed from Eq. (6) relating $q^\mu q_\mu$ to E_1 for E_1 for E held constant at 1200 Mev. It can be shown that the minimum value of $q^\mu q_\mu$ approached at a fixed electron scattering angle and energy E is given by

$$(q^\mu q_\mu)_{\min}=(m/M)[2(1-\cos\theta)]^{\frac{1}{2}}(E^2-M^2). \quad (8)$$

If we neglect the electron rest mass, then in the limit of small secondary electron energy the observed inelastic differential cross section $d^2\sigma/d\Omega dE_2$ is directly related to the pion photoproduction cross section σ_k by purely kinematic and electrodynamic relations. From the analysis of Dalitz and Yennie,[6] we can derive the exact relation

$$\left.\frac{d^2\sigma}{d\Omega dp_2}\right|_{q\mu q_\mu\to 0}=\frac{\alpha}{4\pi^2 E_1}\frac{1}{(1-\cos\theta)}\sigma_k, \quad (9)$$

where α is the fine structure constant. Hence the experimental photopion measurements[4,5] constitute a limiting point to which the measurements off the energy shell have to extrapolate, even though the limit $q^\mu q_\mu\to 0$ cannot strictly be reached physically.

Data have also been taken at fixed momentum transfer and variable E; these reproduce the behavior of the total cross section for photopion reactions.

The dominant term near the photopion resonance involves a magnetic-dipole absorption of the photon when a proton is changed into a neutron; the dominant pion-nucleon final state is then the $T=\frac{3}{2}$, $J=\frac{3}{2}$ state which will govern the relative yields of π^+ and π^0 mesons. The dominant matrix element thus comprises basically three factors: a factor containing kinematic terms, a factor proportional to the difference between the magnetic moments $\mu_p-\mu_n$ of proton and neutron, and the final-state interaction factor which is a function of the pion-nucleon phase shifts. Since we are programming the experiment to keep the energy of the pion-nucleon system constant, the last factor remains constant, and hence the principal unknown is the dependence of $\mu_p-\mu_n$ on the invariant momentum transfer given by Eq. (6). It is in this sense that we interpret this experiment in terms of nucleon-moment form factors.

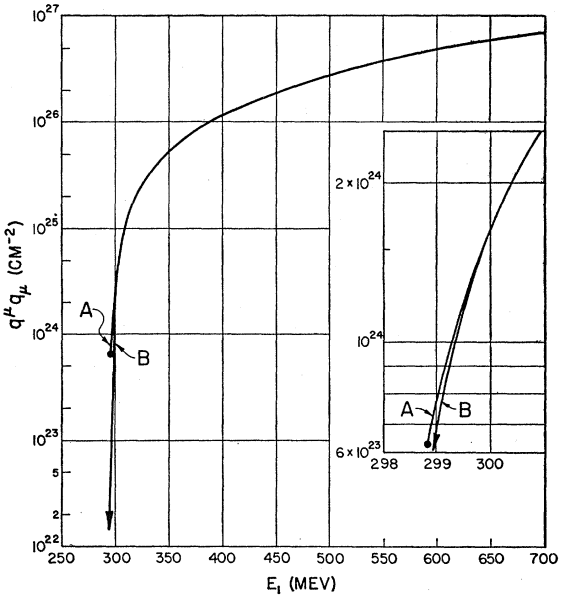

FIG. 3. The invariant momentum transfer $q^\mu q_\mu$ for electron scattering of electrons of finite rest mass m at a fixed scattering angle $\theta=75°$ for a fixed c.m. energy $E=1200$ Mev of the pion-nucleon system, plotted as a function of the initial energy E_1. Curve A is an exact calculation; Curve B is calculated for a zero-rest-mass electron; the insert shows the near-threshold behavior on a larger scale.

II. EXPERIMENTAL PROCEDURES

A. General Arrangement

Figure 4 shows a diagram of the experimental arrangement. A double-magnetic-analyzed[7] electron

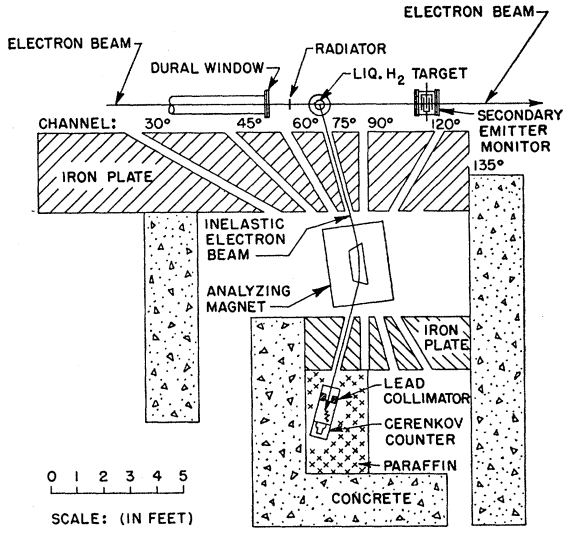

FIG. 4. General experimental arrangement.

[4] Walker, Teasdale, Peterson, and Vette, Phys. Rev. **99**, 210 (1955).
[5] Tollestrup, Keck, and Worlock, Phys. Rev. **99**, 220 (1955).
[6] R. H. Dalitz and D. R. Yennie, Phys. Rev. **105**, 1598 (1957); hereafter referred to as "D-Y."
[7] W. K. H. Panofsky and J. A. McIntyre, Rev. Sci. Instr. **25**, 287 (1954).

TABLE I. Electron-induced processes leading to degraded final electrons other than the processes of Eq. (10) to be studied. Column I lists those reactions in which the initial electron induces reactions in the liquid-hydrogen target leading to final electrons of lesser energy. Column II lists those reactions in which radiative degradation of the primary beam occurs in the material M preceding the target; the final electron is then produced in the target either by γ radiation or the degraded electron.

I. Processes induced by electrons of initial energy in target	II. Two-step processes involving radiation in material (M) preceding target, followed by reaction in target
(A) $e+p\rightarrow e'+p+\gamma$ [large-angle bremsstrahlung]	$e\rightarrow e'+\gamma(M)$ [radiative degradation in M] *followed by* $e'+p\rightarrow e'(\theta)+p$ [Coulomb scattering in target]
(B) $e+p\rightarrow e'+\pi^0+p$; $\pi^0\rightarrow 2\gamma\rightarrow e^-+e^+$ [by conversion or Dalitz pairs[a]]	$e\rightarrow e'+\gamma(M)$ [bremsstrahlung in M] *followed by* $\gamma+p\rightarrow\pi^0+p$; $\pi^0\rightarrow 2\gamma\rightarrow e^-+e^+$ [by conversion or Dalitz pairs[a]]
(C) $e+p\rightarrow e'+\pi^++\pi^-+p$; $\pi^-\rightarrow\mu^-\rightarrow e^-$	$e\rightarrow e'+\gamma(M)$ [bremsstrahlung in M] *followed by* $\gamma+p\rightarrow\pi^++\pi^-+p$; $\pi^-\rightarrow\mu^-\rightarrow e^-$
(D) $e+p\rightarrow e'+e^++e^-+p$ [triplet production]	$e\rightarrow e'+\gamma(M)$ [bremsstrahlung in M] *followed by* $\gamma+p\rightarrow p+e^++e^-$ [large-angle pair production]

[a] R. H. Dalitz, Proc. Phys. Soc. (London) **A64**, 667 (1951).

beam passes through a liquid-hydrogen target and is monitored by a secondary electron monitor.[8] Electrons scattered from the hydrogen are analyzed by a simple wedge magnet employing a 30° deflection. The electrons are detected by a Čerenkov counter containing a liquid of refractive index $n=1.27$.

The liquid-hydrogen target employs a separate liquid-hydrogen reservoir of 2-liter capacity, and a target cell in which hydrogen gas is condensed. The target cell consists of a cylindrical aluminum spinning of 3.5-in. diameter; the cell was spun from 0.020-in. material and was then electropolished to a thickness of 0.006 in. The reservoir loses about one liter in 24 hr in addition to beam energy loss and loss by incomplete ortho-parahydrogen conversion.

B. Competing Processes

Since we want to reduce the results in terms of the cross section of the processes

$$\begin{aligned} e+p &\rightarrow p+\pi^0+e', \\ e+p &\rightarrow n+\pi^++e', \end{aligned} \tag{10}$$

and since the pions are not observed, the question of other processes leading to electrons of reduced energy has to be considered quantitatively.

The possible competing processes are shown in Table I. These reactions have been divided into two classes. Class I contains those reactions in which the primary electron beam produces secondary competing electrons directly on the protons in the hydrogen target. Class II contains those reactions in which a radiative process in the material preceding the target occurs; either the degraded electron or the resultant γ ray produces a secondary electron (or a negative pion difficult to distinguish) in the target material. The various processes are tabulated as (A), (B), (C), (D), by their end products.

We shall now show that, to an excellent degree of approximation, we can eliminate the contribution from all reactions shown in Table I by studying the inelastic electron yield as a function of additional radiating material placed ahead of the target in the incident electron beam.

First let us consider processes I(A) (large-angle bremsstrahlung) and II(A) of Table I. The differential cross section for large-angle bremsstrahlung including all recoil effects can be obtained only as a result of a complex electrodynamic calculation. However, for this purpose the following procedure will suffice: In the limit of infinite nucleon mass the (Bethe-Heitler) cross section contains two separate terms: (a) a term which corresponds to radiation of the initial electron of energy E_1 of a photon essentially parallel to its direction, followed by Coulomb scattering of the resulting electron of energy E_2 through an angle θ; and (b) a term which corresponds to Coulomb scattering of the initial electron of energy E, through an angle θ, followed by emission of a photon essentially parallel to the direction of the final electron. Nucleon recoil, magnetic moment of the nucleon, and finite-size effects can then be introduced as corrections to each of these terms by correcting the relevant Coulomb scattering amplitudes. The integrals of the Bethe-Heitler formula for the two processes have been evaluated from a similar calculation by Schiff.[9] The approximate result is

$$\frac{d^2\sigma}{d\Omega dE_2}=\frac{r_0^2\alpha\mu^2}{4\pi}\left(1+\frac{E_2^2}{E_1^2}\right)\left(\frac{1}{E_1-E_2}\right)\frac{\cos^2(\theta/2)}{\sin^4(\theta/2)} \times\left[\frac{R(E_2)}{E_2^2}+\frac{R(E_1)}{E_1^2}\right]\ln\left(\frac{E_1}{\mu}\right). \tag{11}$$

[8] G. W. Tautfest and H. R. Fechter, Rev. Sci. Instr. **26**, 229 (1955).

[9] L. I. Schiff, Phys. Rev. **87**, 750 (1952).

As pointed out by Schiff,[9] the logarithmic factor is approximate; a more correct factor is $\{\ln[(2E_1/\mu)\times\sin(\theta/2)]-\frac{1}{2}\}$. Here r_0 is the classical electron radius; α is the fine structure constant; and μ is the electron rest energy. The factor $R(E)$ is the recoil and magnetic moment correction which has the form, according to Rosenbluth,[10]

$$R(E)=[1+(2E/M)\sin^2(\theta/2)]^{-1}\times\left\{1+\frac{q^2}{4M^2}[2\mu_p^2\tan^2(\theta/2)+(\mu_p-1)^2]\right\}F^2(q). \quad (12)$$

Here μ_p is the magnetic moment of the proton in units of nuclear magnetons; $q=2E\sin(\theta/2)/[1+(2E/M)\times\sin^2(\theta/2)]^{\frac{1}{2}}$ is the c.m. momentum transfer in the scattering; and $F(q)$ is the electron-scattering form factor[11] to correct for the finite size of the proton.

Equation (11) is plotted in Fig. 5 for those parameters chosen in the basic experiment, namely that relation between E_2 and E_1 corresponding to an energy $E=1200$ Mev of the meson-nucleon system according to Eq. (4) if the scattering angle θ is 75°.

Note that Eq. (11) can be written in the simple form

$$\sigma_{\rm I}=\frac{d^2\sigma}{d\Omega dE_2}=\left[\frac{\alpha}{\pi}\left(1+\frac{E_2^2}{E_1^2}\right)\ln\left(\frac{E_1}{\mu}\right)\right]\frac{1}{E_1-E_2}\times\left[\frac{d\sigma}{d\Omega}(E_1)+\frac{d\sigma}{d\Omega}(E_2)\right], \quad (13)$$

where $d\sigma(E)/d\Omega$ is simply the elastic electron-proton scattering cross section. The fact that (11) contains the elastic cross sections in factorable form implies that the electron in the intermediate state in the two diagrams governing the bremsstrahlung process is essentially real.

Now let us consider process II(A) of Table I (radiative degradation of the electron prior to scattering, followed by elastic scattering). Let the radiative degradation occur in t radiation lengths of material. The effective cross section due to this process is then given by

$$\sigma_{\rm II}=\frac{d^2\sigma}{d\Omega dE_2}=\frac{t'}{E_1-E_2}\cdot\frac{d\sigma}{d\Omega}(E_2), \quad (14)$$

where

$$t'=t[kN(k)]; \quad (15)$$

here $N(k)dk$ is the number of photons emitted per radiation length of radiator between energy k and $k+dk$. By the definition of radiation length, $kN(k)\approx 1$ or $t'\approx t$.

In Eq. (13),

$$\frac{d\sigma}{d\Omega}(E_1)\ll\frac{d\sigma}{d\Omega}(E_2). \quad (16)$$

[10] M. N. Rosenbluth, Phys. Rev. **79**, 615 (1950).
[11] E. E. Chambers and R. Hofstadter, Phys. Rev. **103**, 1454 (1956).

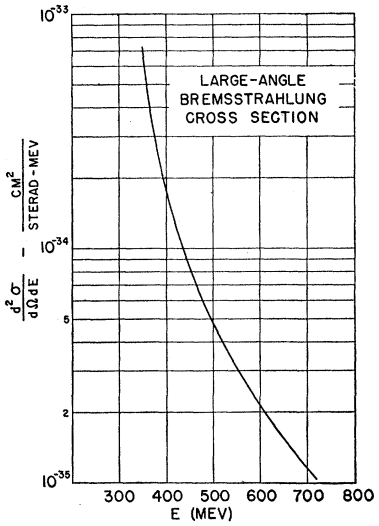

FIG. 5. Plot of the cross section for inelastic scattering of electrons of energy E_1 with the emission of bremsstrahlung leading to a final electron of energy E_2 at an angle of 75°. The cross section is plotted as a function of E_1 for that relation between E_1 and E_2 required by Eq. (6) for $E=1200$ Mev.

To a good approximation we can neglect $d\sigma(E_1)/d\Omega$; Eqs. (13) and (14) then have the same form; both processes are equivalent if we describe the large-angle bremsstrahlung by radiative degradation from an electron energy E_1 to an energy E_2, equivalent to that produced by a physical radiator of radiation length

$$N_B=(\alpha/\pi)[1+(E_2^2/E_1^2)]\ln(E_1/\mu), \quad (17)$$

followed by elastic scattering.

This analysis suggests the following procedure to eliminate the background due to both processes I(A) and II(A). Let us observe the count C^- under standard conditions where only a minimal amount of material of equivalent radiation length t_j' is in the beam. Then add a radiator of equivalent radiation length t_R' and observe the new increased count C_R^-. The corrected count C_C^- obtained by the simple proportionality

$$C_C^-=C^--(C_R^--C^-)[(N_B+t_j')/t_R'] \quad (18)$$

extrapolates the count to zero total (real plus effective) radiator thickness, and therefore will evidently not contain the contribution of either process I(A) or II(A); we have used the increase in count due to the radiator as a means of measuring the processes in question.

We shall now show that this same procedure serves to eliminate the contributions from the pion processes (B) and (C) of Table I, whether these are induced by real or virtual photons. As we have shown in our previous papers,[1-3] electron-induced pion production can be represented by an equivalent radiation length N_e; this is defined such that pion production by bremsstrahlung produced by electrons in a real radiator of radiation length N_e is equal to that produced by direct production by the electrons via virtual photons.

Theoretical values of N_e have been discussed extensively in D-Y. For purposes of these corrections the value of N_e for magnetic-dipole absorption given by

$$N_e=(\alpha/\pi)[1+(E_2^2/E_1^2)]\ln[2E_2E_1/\mu(E_1-E_2)] \quad (19)$$

is of sufficient accuracy. Computation shows that N_e given by Eq. (19) and N_B given by Eq. (17) are equal to within 10% over the range of variables of interest. Hence the extrapolation formula (18) also eliminates the contributions from all pions and pion decay products.

A similar argument applies qualitatively to the pair processes (D); however, these are two orders of magnitude lower in yield in comparison with (A), (B), and (C).

A sharp test of the validity of the extrapolation procedure represented by Eq. (18) is provided by observing positive secondary particles at rates C^+ and $C_R{}^+$, either without or with additional radiator. If the considerations above are valid, then the extrapolated count

$$C_C{}^+=C^+-(C_R{}^+-C^+)(N_e+t_j')/t_R' \quad (20)$$

should vanish within the statistical accuracy of the data. Our later discussion of the results shows that this is indeed so. This test is the more significant since the process $\gamma+p\rightarrow\pi^++n$ leads to an additional copious source of positrons beyond those originating from the processes tabulated in Table I.

There are thus two procedures for reducing the data of this experiment: *Procedure* I: Observe C^-, $C_R{}^-$, C^+, $C_R{}^+$, and calculate $C_C{}^-$ by extrapolation using Eq. (18); check $C_C{}^+$ according to Eq. (20). *Procedure* II: Observe C^- and correct the data directly by the known cross sections (13) and (14); this procedure, since it clearly neglects processes (B)–(D) of Table I, gives an upper limit on the cross sections; owing to the lack of an extrapolation procedure the statistical accuracy is higher. Procedures I and II are expected to agree in the region of high secondary electron energies where the π^0 contributions are small; this is verified by the data.

C. Normalization of Data

The detection apparatus outlined in Sec. IIA does not permit the measurement of absolute cross sections. We thus chose to normalize the measurements against the well-established[11] cross section $d\sigma_e/d\Omega$ for elastic electron scattering. This normalization occurs in regions of electron energy where the form factors[11] are close to unity; hence no significant uncertainty exists in the values of the reference cross section.

The procedure adopted here in comparing the measured counts in the continuous inelastic spectrum corresponding to an inelastic cross section $d^2\sigma_i/d\Omega dE_2$ is designed to minimize errors depending on the performance of the analyzing spectrometer.

In the execution of the experiment we take two kinds of data: (1) inelastic counts $C_i(E_S,E_M)$ taken when the slit selector system of the primary analyzer is "set" at E_S and when the secondary-particle analyzer is "set" at E_M, and (2) elastic counts $C_e(E_S,E_M)$ taken under similar conditions but when E_S and E_M are near the values connected by the equation

$$E_2=f(E_1)=E_1[1+(E_1/M)(1-\cos\theta)]^{-1}, \quad (21)$$

describing the kinematics of elastic electron scattering. Let the number dN of primary electrons between energies E_1 and E_1+dE_1 passing through the primary analyzing system be given by

$$dN=\frac{N}{E_S}S\left(\frac{E_1-E_S}{E_S}\right)dE_1, \quad (22)$$

where N is the total number of electrons and S describes the incident electron spectrum.

Let the over-all detection efficiency of the analyzer at "setting" E_M be given by

$$\epsilon(E_2)=\eta(E_2)R\left(\frac{E_2-E_M}{E_M}\right), \quad (23)$$

where $\eta(E_2)$ is the efficiency of the final counter system. Analysis shows that C_i, $(d^2\sigma_i/d\Omega dE_2)$, C_e, and $(d\sigma_e/d\Omega)$, are related by

$$C_i(E_S,E_M)=N\int\int\frac{1}{E_S}S\left(\frac{E_1-E_S}{E_S}\right)\frac{d^2\sigma}{d\Omega dE_2}\times\eta(E_2)R\left(\frac{E_2-E_M}{E_M}\right)dE_1dE_2, \quad (24)$$

and

$$C_e(E_S,E_M)=N\int\frac{1}{E_S}S\left(\frac{E_1-E_S}{E_S}\right)\frac{d\sigma}{d\Omega}\times\eta(E_2)R\left(\frac{E_2-E_M}{E_M}\right)dE_1, \quad (25)$$

where, in (25), E_1 and E_2 are related by Eq. (21). If the primary spectrum S is narrow compared to the secondary resolution R, then it can be shown from (21), (24), and (25) that

$$\frac{d^2\sigma}{d\Omega dE_2}(E_S,E_M)=C_i(E_S,E_M)\Big/\int\frac{C_e(E_S',E_M)}{d\sigma(E_S')/d\Omega}f'(E_S')dE_S'. \quad (26)$$

Hence in the actual execution of the experiment we take the count $C_i(E_S,E_M)$ and then vary E_S, the primary machine energy, near values demanded for elastic scattering into an energy E_M; $C_e(E_M,E_S)$ is then a typical "elastic curve" used for reference. Note that the configuration for the detection of the electrons E_2 remains the same during the observation of C_i and C_e; this method is thus totally independent of the

behavior of the detecting system as to variation of efficiency with energy, slit scattering, radiative degradation after scattering, etc. In practice, it is not possible to carry out the integration,

$$I(E_M)=\int_0^L \frac{C_e(E_S',E_M)f'(E_S')}{d\sigma(E_S')/d\Omega}dE_S', \qquad (27)$$

in the denominator of (24) to arbitrarily large values of L; we have chosen $L=(5/4)E_S$ in our computation; this means that if the primary beam is radiation-straggled by an equivalent radiation length t_j', then a fraction

$$t_j' \ln\left(\frac{E_S}{L-E_S}\right)=1.39t_j' \qquad (28)$$

is lost to the integral. This amount can be added to Eq. (27) as a correction to a good degree of approximation. The loss of count due to radiation straggling of the scattered electrons is less important.

The normalization procedure outlined above makes absolute current measurements unnecessary. Nevertheless we have to assume that the readings of the secondary electron monitor[8] are sufficiently energy-independent. Tautfest and Fechter[8] carried out tests up to an electron energy of 300 Mev and found the energy variation of the response of a particular instrument to be less than 0.7% in the range 100 Mev$<E<$250 Mev. We have continued these tests up to an energy of 600 Mev by comparing the charge collected on the secondary-emission monitor with that collected on a large Faraday cup. This cup was designed by J. A. McIntyre to contain the entire shower produced by a 600-Mev electron with a charge loss of less than $\frac{1}{2}$%; it has been used as a monitor by the electron-scattering group at this laboratory. Its performance as to small side effects (such as collection of secondary electrons from the entrance foil) has not as yet been evaluated. We found that in the range of energies 300 Mev$<E<$600 Mev the collection efficiency of the secondary-electron monitor relative to the Faraday cup increased linearly from 2.82 to 3.12%. This apparent increase of the sensitivity of the secondary-electron monitor may be due to a residual error in the Faraday cup. Applying this energy variation to our calculated cross sections, we find a correction of +11% to the point taken at $E_1=700$ Mev, and a correction of +9% to the point at $E_1=400$ Mev, with corresponding corrections for the intermediate points; the need for these corrections is dubious.

We have also examined the effect of placing a radiator in the beam on the efficiency of the monitor, and found the effect to be negligible.

D. Energy Calibration

The energy of the primary beam is defined by a collimator and slit system described previously.[7] These were calibrated by the floating-wire technique. Energy values above 100 Mev are believed accurate to better than 1%. The analyzer was calibrated by the floating-wire technique also. The consistency between the two calibrations was checked by the position of the "elastic peaks." Figure 6 shows values of E_2 chosen in this experiment as measured by the floating-wire technique and as inferred from the primary energy. Figure 6 also shows the kinematic relations between E_1, E_2, and E. It is clear from the consistency of the points that the value of E is not likely to deviate from the design value of 1200 Mev by more than ±10 Mev.

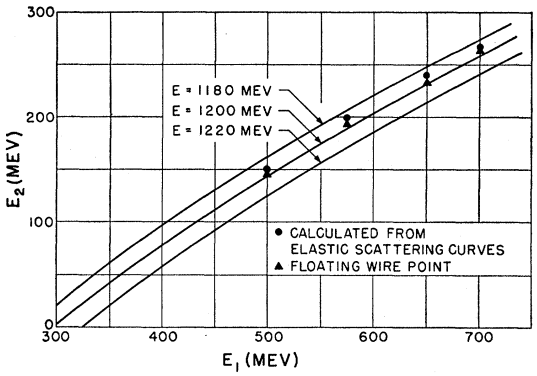

FIG. 6. Values of initial electron energy E_1 and final electron energy E_2 as actually used in this experiment to correspond to a c.m. energy $E=1200$ Mev. Values of E_2 plotted correspond to (a) the nominal setting of the magnetic analyzer as calibrated by the floating-wire method, and (b) the value computed from the peak of the elastic-scattering curves as calculated from the primary energy calibration and Eq. (21). Also shown are the kinematic relations between E_1 and E_2 for c.m. energies of $E=1180$, 1200, and 1220 Mev. This figure thus documents the consistency of the initial and final electron energy calibrations.

III. RESULTS

A. Tabulation of Data

Figure 7 shows a three-dimensional plot giving the values of $d^2\sigma/d\Omega dE_2$ measured as a function of the c.m. energy E and the invariant momentum transfer $q^\mu q_\mu$. Three classes of measurement are shown: (1) measurements taken at "resonance" at a constant value of $E=1200$ Mev; (2) measurements taken at a constant value of momentum transfer $[q^\mu q_\mu \cong 1.4\times 10^5 (\text{Mev}/c)^2]$ but variable energy; (3) a curve at $q^\mu q_\mu=0$, computed from experimental photoproduction data by means of Eq. (9). Our conclusions are based primarily on the first class of measurements. Figure 7 serves primarily to illustrate the relation of these measurements to the photoproduction data.

Tables II and III give a summary of our data. Included in these tables are the following entries: C^-, counts with negative analyzer, no additional radiator; C_R^-, counts with negative analyzer, an additional copper radiator of 0.476 g/cm^2, corresponding to a value of $t'=0.0336$ effective radiation length; C^+, counts with positive analyzer, no additional radiator;

TABLE II. Primary data. Shown are (1) the initial and final electron energies; (2) the c.m. energy E of the pion-nucleon system and the invariant momentum transfer; (3) the observed counts for analyzer magnet settings of either sign and with and without additional radiator; (4) the normalizing integral $I(E_M)$, and $I(E_M)_{\text{corr}}$ as corrected for radiation-tail cutoff and monitor calibration.

	E_1 (Mev)	E_2 (Mev)	E (Mev)	$q^\mu q_\mu$ (cm^{-2} $\times 10^{-26}$)	C^-	C_R^- (counts/(2.0 $\times 10^{14}$ electrons))	C^+	C_R^+	$\left(\frac{I(E_M)\ I(E_M)_{\text{corr}}}{\text{counts}\times\text{Mev}\times 10^{35}}{2\times 10^{14}\text{ electrons}\times(\text{cm}^2/\text{sterad})}\right)$	
Constant E runs	700	262	1200	6.93	21.6±1.2	28.7±1.4	...	...	2.02	1.85
	650	235	1200	5.75	26.9±1.0	33.0±1.0	6.67±0.53	16.6±0.8	1.76	1.61
	575	192	1200	4.13	39.1±1.3	47.4±1.4	11.0 ±0.70	21.4±0.9	1.62	1.50
	500	145	1200	2.75	47.9±0.9	70.4±1.1	12.8 ±0.8	25.3±1.2	1.17	1.09
	400	78	1200	1.13	73.8±2.7	128 ±3.1	31.7 ±2.0	67.5±2.6	0.647	0.617
Constant momentum-transfer runs	440	215	1080	3.46	27.3±1.4	46.1±1.8	...	...	2.09	1.97
	488	193	1135	3.46	30.2±1.7	45.1±2.1	...	...	1.70	1.60
	650	144	1300	3.46	34.6±1.3	62.0±1.8	...	...	1.17	1.06
	700	133	1340	3.46	32.9±1.3	59.0±1.7	...	...	(1.17)	1.04

C_R^+, counts with positive analyzer, additional radiator as given above; $I(E_M)$, the integral of Eq. (27); σ^-, σ_R^-, σ^+, σ_R^+, the counts C^-, C_R^-, C^+, and C_R^+ normalized by $I(E_M)$ and corrected for (a) counts lost by radiation [Eq. (28)] and (b) energy sensitivity of the monitor; σ_C^-, and σ_C^+, the cross sections corresponding to the desired process by eliminating the contribution of the processes of Table I by means of Eqs. (18) and (20); and $(\sigma^-)_{\max}$, the "upper-limit" cross section obtained by subtracting the calculated contributions σ_{I} and σ_{II} from large-angle bremsstrahlung and Coulomb scattering of degraded electrons, Eqs. (13) and (14), from σ^-.

We can draw the following conclusions by inspection of this table: (a) The values of σ_C^+ vanish within statistics; the sum of all the corrected cross sections σ_C^+ calculated from Eq. (20) is $(0.028\pm0.064)\times10^{-34}$ cm^2/Mev-sterad. (b) For the larger values of E_1 and E_2 the upper-limit cross sections $(\sigma^-)_{\max}$ are only slightly above the extrapolated cross sections σ_e^-; at lower values the difference widens; this is due to the neglect of the π^0 contribution in calculating the "upper limit" cross section $(\sigma^-)_{\max}$.

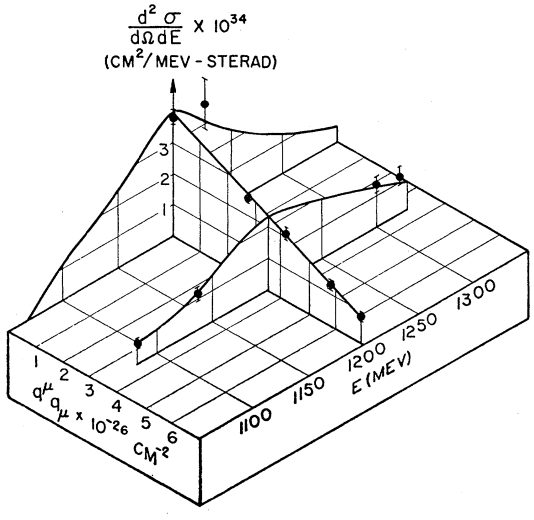

FIG. 7. Three-dimensional isometric plot of the experimental data. Plotted are the measured cross sections $d^2\sigma/d\Omega dE_2$ *vs* the c.m. energy E and the invariant momentum transfer $q^\mu q_\mu$. The points in the $q^\mu q_\mu=0$ plane are computed from experimental photoproduction data.

B. Comparison with Pion Photoproduction Data

The results for σ_C^- have been plotted on the three-dimensional (isometric) representation Fig. 7. The values of σ_C^- and $\sigma_{\max}^-$ for $E=1200$ Mev are also shown in Fig. 8 plotted against the values of the invariant momentum transfer, Eq. (7). Plotted on both figures are the values for $q^\mu q_\mu\to0$ as computed from photoproduction data. The photoproduction values adopted are $\sigma_{\pi^0}=2.50\times10^{-28}$ cm^2 at $k=298$ Mev ($E=1200$ Mev); $\sigma_{\pi^+}=2.06\times10^{-28}$ cm^2 at $k=298$ Mev ($E=1200$ Mev). Hence, from Eq. (9),

$$\lim_{q^\mu q_\mu\to0}\left(\frac{d^2\sigma}{d\Omega dE_2}\right)=(3.81\pm0.30)\times10^{-34}\text{ cm}^2\text{ sterad}^{-1}\text{ Mev}^{-1}. \quad (29)$$

We have found it somewhat difficult to assign a probable error to this figure. The values quoted are means of the measurements made at the California Institute of Technology[4,5]; it is well-known[12] that the analysis of photoproduction data by dispersion theory[13,14] gives an excellent fit[15] to π^0-production cross sections, but that the fit for π^+ production is less satisfactory. If the same coupling constant is used for the S- and P-wave terms, then the π^+ cross section at resonance exceeds the experimental value if the coupling constant is chosen in accordance with the π^0 results.

The "quartic analysis" of Moravcsik[16] does not add

[12] See the report by E. L. Goldwasser, *Proceedings of the Seventh Annual Rochester Conference on High-Energy Nuclear Physics* (Interscience Publishers, Inc., New York, 1957), pp. II-50 ff.

[13] Chew, Goldberger, Low, and Nambu, Phys. Rev. **106**, 1345 (1957), and earlier papers cited there.

[14] A. A. Saganov and B. M. Stepanov, Doklady Akad. Nauk S.S.S.R. **110**, 3 (1956).

[15] L. J. Koester and F. E. Mills, Phys. Rev. **105**, 1900 (1957).

[16] M. J. Moravcsik, Phys. Rev. **107**, 600 (1957). We are indebted to Dr. Moravcsik for helpful correspondence concerning the uncertainties of his data-fitting procedures.

TABLE III. The observed cross sections. The cross sections corresponding to the various counts of Table II are shown. Given also are the cross sections extrapolated to zero-radiator thickness by Eqs. (18) and (20) for negative and positive settings; the column σ_C^- thus represents the final cross sections. The last columns give the theoretical [Eq. (13)] large-angle bremsstrahlung cross sections and the upper-limit cross sections $(\sigma^-)_{max}$ calculated by subtracting the large-angle bremsstrahlung cross sections and the Coulomb scattering from degraded-electrons from the uncorrected cross sections σ^-.

	E Mev	$q_\mu q^\mu$ (cm^{-2}) $\times 10^{-26}$	σ^-	σ_R^-	σ^+	σ_R^+	σ_C^-	σ_C^+	σ_B	$(\sigma^-)_{max}$
			[cm^2/(sterad-Mev)] $\times 10^{34}$						[cm^2/(sterad-Mev)] $\times 10^{34}$	
Constant E runs	1200	6.93	1.17±0.06	1.55±0.08	...	...	0.82±0.13	...	0.197	0.97±0.06
	1200	5.75	1.67±0.07	2.05±0.07	0.413±0.03	1.03±0.05	1.33±0.14	−0.165±0.08	0.270	1.40±0.07
	1200	4.13	2.61±0.09	3.16±0.09	0.728±0.05	1.43±0.06	2.10±0.19	0.09 ±0.11	0.458	2.15±0.09
	1200	2.75	4.40±0.08	6.47±0.10	1.17 ±0.07	2.32±0.11	2.57±0.16	0.19 ±0.48	0.875	3.52±0.08
	1200	1.13	11.9 ±0.4	20.8 ±0.5	5.06 ±0.3	10.8 ±0.4	4.8 ±0.8	0.38 ±0.56	2.22	9.2 ±0.4
Constant momentum-transfer runs	1080	3.46	1.39±0.07	2.34±0.09	...	...	0.61±0.15	...	...	...
	1135	3.46	1.89±0.11	2.81±0.13	...	...	1.17±0.24	...	...	...
	1300	3.46	3.26±0.12	5.85±0.17	...	...	1.35±0.25	...	...	...
	1340	3.46	3.16±0.13	5.68±0.16	...	...	1.16±0.27	...	...	...

substantially to the accuracy of computation of the total cross section over the earlier two-coefficient fits used by the original experimenters.[4,5] The values adopted above thus ignore the theoretical incompleteness of the fit of the data to photoproduction data. We are thus considering the point as given in Eq. (29) as being an *experimental* point contributed by the California Institute of Technology work[4,5] to our data.

IV. ANALYSIS OF FORM FACTORS

The matrix elements for pion photoproduction contain the following primary terms: (a) magnetic-dipole

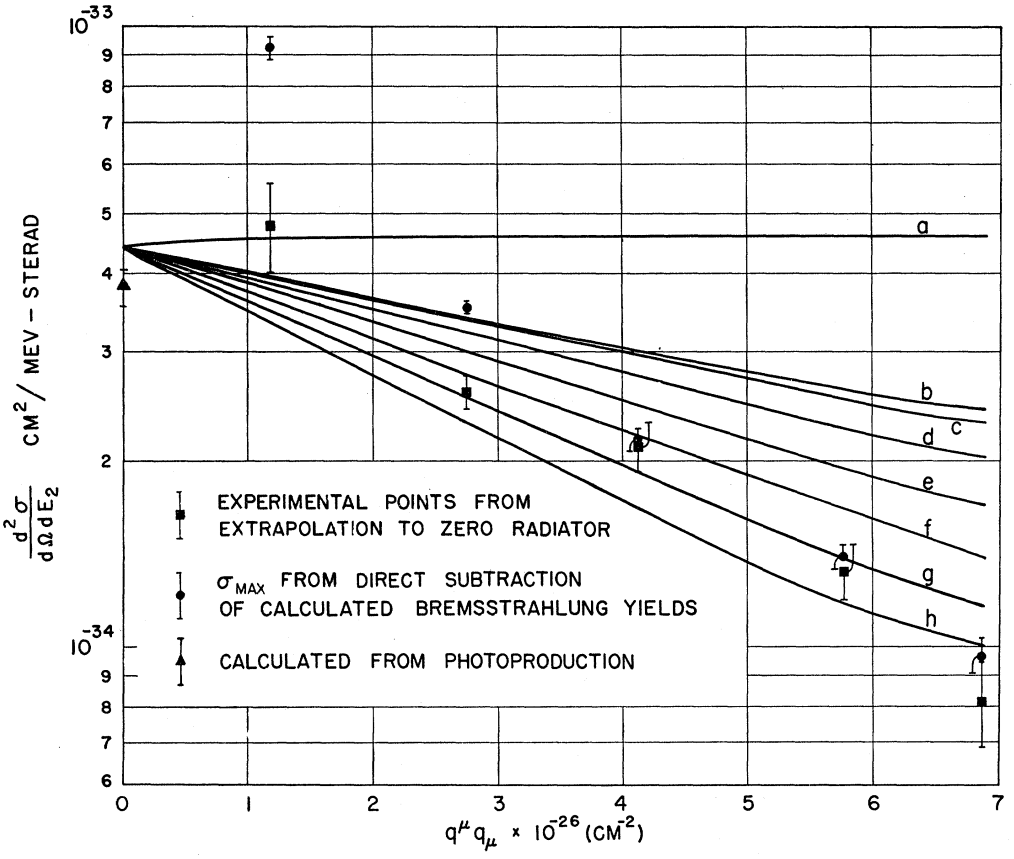

FIG. 8. Experimental data obtained at constant c.m. energy $E=1200$ Mev plotted against the invariant momentum transfer. Shown are both the extrapolated cross sections σ_e^- and upper-limit cross sections $(\sigma^-)_{max}$. These measurements are compared with the following theoretical curves: (a) point interaction; (b) a_p=electric and magnetic proton radius$=0.8\times10^{-13}$ cm, a_n=magnetic neutron radius$=0$; (c) $a_p=0.8\times10^{-13}$ cm, $a_n=0.2\times10^{-13}$ cm; (d) $a_p=0.8\times10^{-13}$ cm, $a_n=0.4\times10^{-13}$ cm; (e) $a_p=0.8\times10^{-13}$ cm, $a_n=0.6\times10^{-13}$ cm; (f) $a_p=0.8\times10^{-13}$ cm, $a_n=0.8\times10^{-13}$ cm; (g) $a_p=0.8\times10^{-13}$ cm, $a_n=1.0\times10^{-13}$ cm; (h) $a_p=0.8\times10^{-13}$ cm, $a_n=1.2\times10^{-13}$ cm. Radii are rms values based on an exponential model.

absorption leading to the final "resonant" $(\frac{3}{2},\frac{3}{2})$ state of the nucleon-meson system; (b) electric-dipole absorption leading to a final S state of the pion-nucleon system; (c) the "direct interaction" term of the photon with the virtual meson cloud surrounding the nucleus calculated in Born approximation. Neutral-pion production is concerned with the first term (a) only; assuming charge independence, term (a) contributes half as much to positive-pion production as to neutral-pion production. Since at the c.m. energy $E=1200$ Mev used here the neutral and charged cross sections are approximately equal, we conclude that roughly three fourths of the measurements reported here come from the "resonant" term (a); "off the energy shell" the relative contribution of the (a) term becomes still larger.

The primary interpretation of this work will thus be in terms of the nuclear form factor associated with term (a), which is the form factor associated with $\mu_p-\mu_n$. This interpretation is singularly insensitive to a particular choice of constants of a specific theoretical fit since the form factors depend only on the relative cross sections as a function of momentum transfer; constants have to be chosen to agree with experiment on the energy shell; as long as the magnetic-dipole term is dominant, the details of handling the other terms are unimportant.

In the more detailed analysis we have followed the dispersion theoretical analysis of photoproduction by Chew *et al.*[13] extended to the electron-pion process by Fubini, Nambu, and Wataghin.[17] Unfortunately, their analysis is not complete with respect to the inclusion of kinematic nucleon recoil terms; some of the quantitative conclusions can thus be improved as soon as further calculations have been completed.

It was shown by FNW that the electric-dipole absorption term (b) involves the electric form factor (F_1 in the notation of Hofstadter[18] and collaborators); the appropriate factor here involves the difference between the electric form factors of the proton and neutron. Since the neutron's charge and its second moment vanish (as concluded from the low-energy electron-neutron interaction), we have used simply the F_1 factor appropriate to the proton in computing the electric-dipole term, thus assuming the electric form factor of the neutron to vanish even for large momentum transfers. For the reasons enumerated above, we are not sensitive to this assumption; however, further work of this nature, in which the kinematic relations are programmed to emphasize the electric-dipole term, should have important bearing on this question.

The analysis of FNW contains several small terms other than the large contributions (a), (b), and (c), discussed above. These contain the appropriate electric or magnetic form factors linearly or quadratically, depending on whether the terms are interference terms or not. These form factors have been included in the computation treating the magnetic radius of the neutron as a variable, letting the electric radius of the neutron vanish, and taking the electric and magnetic radius of the proton as 0.8×10^{-13} cm rms.

Figure 8 shows our experimental data [both the extrapolated cross section σ_C^- and the upper-limit cross section $(\sigma^-)_{\max}$ of Table II] plotted on a logarithmic scale against the invariant momentum transfer $q^\mu q_\mu$ (λ^2 in the notation of FNW). The various terms from FNW have been computed by C. Lindner with the collaboration of S. Gartenhaus; the authors are greatly indebted to them for their contributions. The same renormalized coupling constant ($f_r^2=0.090$) was used for all terms in the matrix elements; this gives a reasonable fit to the magnitudes of the neutral-pion cross sections, while the experimental charged-pion cross section is somewhat low; as discussed above, the conclusions are insensitive to the choice of this number. Using the computed terms, we have plotted a number of theoretical curves showing the dependence of the cross sections on various nucleon structure parameters. The following curves are shown: Curve (a), all form factors unity, i.e., all nucleons are points. Curves (b)–(h), the form factor of the electric-dipole term equal to the electric form factor F_1 of the electron-proton scattering results[11,18] has been used as discussed above. The magnetic moment of the proton has been multiplied by the appropriate magnetic form factor F_2; the magnetic moment of the neutron has been multiplied by a set of form factors corresponding to various radial parameters. We have computed the form factors using an exponential radial distribution whose Fourier transform is $[1+(q^\mu q_\mu a^2/12)]^{-2}$, where a is the rms radius. We have used $a_p=0.8\times10^{-13}$ cm for both the electric and magnetic form factors of the proton, in accordance with the electron-scattering results. Unfortunately, the accuracy for small values of the momentum transfers is poor (and is very difficult to improve); hence we are unable to analyze the results in terms of an rms radius without assuming a specific form of distribution. We have used here the exponential model in order to permit comparison with the parameters obtained from elastic electron scattering on the proton and quasi-elastic scattering on the deuteron.[19]

By inspection of Fig. 8 we see that a best fit is obtained for values of a_n between 1.0×10^{-13} and 1.1×10^{-13} cm for the rms neutron magnetic radius, based on the exponential model. The experimental values permit little latitude toward smaller values since the upper-limit cross section $(\sigma^-)_{\max}$ agrees with the extrapolated value at large momentum transfers.

[17] Fubini, Nambu, and Wataghin, Phys. Rev. (to be published); hereafter called "FNW." Dr. Fubini acquanted us with this work in the summer of 1957, and Professor Nambu discussed some of the problems associated with the nucleon recoil contributions in December, 1957.

[18] R. Hofstadter, Revs. Modern Phys. **28**, 214 (1956).

[19] M. R. Yearian and R. Hofstadter, Phys. Rev. (to be published).

The principal remaining uncertainty relates to the treatment of nucleon recoil terms in the off-the-energy-shell behavior of the magnetic-dipole absorption matrix element. We have been assured[20] that such recoil terms are not fundamentally ambiguous and are subject to calculation. Until such calculations have been performed, we would consider a value of the rms magnetic radius of the neutron as low as 0.8×10^{-13} cm to be compatible with the data.

We should like to add that the experimental method described here has much more general validity beyond the limited range of electron variables explored. In particular, a more complete mapping of the surface of Fig. 7 is being planned. If higher energy electron beams are available, the electromagnetic production mechanism of particles other than the pion can be studied by similar methods.

ACKNOWLEDGMENTS

We are pleased to acknowledge the valuable collaboration of many members of this laboratory in connection with this experiment. A. Grubman and E. A. Wright gave necessary assistance with the liquid-hydrogen target; J. Pope developed the difficult electropolishing technique to produce a liquid-hydrogen cell of well-defined geometry, thin wall thickness, and capable of withstanding intense electron bombardment. The experiment imposed severe requirements on the operation of the accelerator, including reliable operation at 700 Mev; these demands were met by the accelerator operating group under the direction of R. G. Gilbert. We gratefully acknowledge the collaboration of G. B. Yodh in the early planning of the experiment, and the assistance of R. Alvarez, F. Bulos, K. Brown, L. Becker, F. Bumiller, and A. Lazarus during data-taking runs.

Our theoretical understanding of this problem was substantially improved by discussions with Dr. Yennie, Dr. Fubini, Dr. Nambu, and Dr. Gartenhaus; in addition, we gratefully acknowledge the specific contributions of Dr. Gartenhaus and of C. Lindner. We are also grateful to Professor R. Hofstadter and to M. Yearian for keeping us informed on the progress of their work on quasi-elastic electron scattering on the deuteron and its interpretation in terms of the magnetic form factor of the neutron. We also thank Dr. Burton Richter for his help in handling the spectrometer resolution problem.

[20] Y. Nambu (private communication).